NOVEL COUMARINS AND RELATED COPPER COMPLEXES WITH BIOLOGICAL ACTIVITY: DNA BINDING, MOLECULAR DOCKING AND IN VITRO ANTIPROLIFERATIVE ACTIVITY

Tiziana Pivetta[a#], Elisa Valletta[a], Giulio Ferino[b,c], Francesco Isaia[a], Alessandra Pani[d], Sarah Vascellari[d], Carlo Castellano[e], Francesco Demartin[e], Maria Grazia Cabiddu[a], Enzo Cadoni[a]

[a]Dipartimento di Scienze Chimiche e Geologiche, Università degli Studi di Cagliari, Cittadella Universitaria di Monserrato, 09042 Monserrato (CA) – ITALY; [b]Centro Screening Neonatale, Ospedale Pediatrico A.Cau, Azienza Ospedaliera Brotzu, Via Jenner, Cagliari; [c]Dipartimento di Salute Pubblica, Medicina Clinica e Molecolare, Università degli Studi di Cagliari, Cittadella Universitaria di Monserrato, 09042 Monserrato (CA) – ITALY; [d] Dipartimento di Scienze Biomediche, Università degli Studi di Cagliari, Cittadella Universitaria di Monserrato, 09042 Monserrato (CA) – ITALY, [e] Dipartimento di Chimica, Università degli Studi di Milano, via Golgi, 19 20133 Milano

corresponding author tpivetta@unica.it, +39 070 675 4473

Keywords: coumarin, anticancer, copper complexes, DNA binding, molecular docking, QSAR

Abstract

Coumarins show biological activity and are widely exploited for their therapeutic effects. Although a great number of coumarins substituted by heterocyclic moieties has been prepared, few studies have been carried out on coumarins containing pyridine heterocycle, which is known to modulate their physiological activities. We prepared and characterised three novel 3-(pyridin-2-yl)coumarins and their corresponding copper(II) complexes. We extended our investigations also to three known similar coumarins, since no data about their biochemical activity was previously been reported. The antiproliferative activity of the studied compounds was tested against human derived tumour cell lines and one human normal cell line. The DNA binding constants were determined and docking studies with DNA carried out. Selected Quantitative Structure-Activity Relationship (QSAR) descriptors were calculated in order to relate a set of structural and topological descriptors of the studied compounds to their DNA interaction and cytotoxic activity.

1. Introduction

Coumarins, belonging to the benzo-alfa-pyrones family [1], show biological activity and are studied for their therapeutic effects. In nature, coumarins are found in higher plants like Rutaceae and Umbelliferae [2]. Umbelliferone, esculetin and scopoletin are very common coumarins found in the plant kingdom. Coumarins are also found in Streptomycin and Aspergillus microorganisms [3]. Due to their biochemical and physical properties, coumarins are used as enhancing agents in cosmetic products [4], fluorescent probes, markers for biological research [5] and as drugs [6] in medicine for the treatment of various clinical conditions [7], including as anti-inflammatory [8,9], antimicrobial [10], antioxidant [10,11], anticouagulant [12] and anticancer [8] drugs. As regards this last aspect, coumarins and derivatives have been used in the treatment of solid [13-19] and liquid [20] cancers to exploit their ability to act with different mechanisms related to their chemical structure [1]. In fact, the biochemical, pharmacological and therapeutic properties of coumarins can be tuned by the substitution or inclusion of a heterocyclic moiety as a substituent or as a fused component in the

coumarin backbone [3]. Although a great number of coumarins substituted by heterocyclic moieties has been prepared, few studies have been carried out on those containing a pyridine heterocycle [21,22], known to modulate the physiological activities [23-25] of coumarins. In order to develop effective and non-toxic new drugs, several metal-coumarin complexes have also been prepared [26-29] and some show a biological activity higher than that of coumarin itself [30,31].

With the aim of preparing new drugs with anticancer activity, we prepared and characterised three novel 3-(pyridin-2-yl)coumarins derived from substituted salicylaldehydes and 2-pyridylacetonitrile (Fig. 1, **L2**-**L4**). We extended our study also to three known similar coumarins (Fig. 1, **L1**, **L5**, **L6**), since no investigations about their biochemical activity have been reported. The crystal structures of **L1·HClO$_4$**, **L4** and **L6** were solved by single crystal X-ray diffraction. Copper complexes with the six coumarins were also prepared. Copper was chosen as several copper complexes show antiproliferative activity [31-35].

The antiproliferative activity of all the compounds has been tested against human derived tumour cell lines, i.e. human acute T-lymphoblastic leukaemia (CCRF-Cem), human acute B-lymphoblastic leukaemia (CCRF-Sb), human lung carcinoma (Sk-Mes 1), human prostate carcinoma (Du 145), human hepatocellular carcinoma (Hep-G2) and human normal foreskin (CRL 7065).

As DNA is an important target for several anticancer drugs, its binding constants have been determined. Moreover, to understand the interactions of the prepared coumarins and complexes with DNA and the orientation of these molecules at the active site of the DNA, docking studies were carried out. Selected quantitative structure-activity relationship (QSAR) descriptors were calculated in order to relate a set of structural and topological descriptors of the studied compounds to their DNA interaction and biological activity.

2. Results and discussion

2.1 Synthesis and characterization of ligands

The derivatives of 3-(pyridin-2-yl)coumarins were prepared from substituted salicylaldehydes and 2-pyridylacetonitrile via Knoevenagel condensation [36]. The resulting 2-iminocoumarins were converted to coumarins by acid hydrolysis of the imines (Scheme 1).

Ligands were characterized by ^{1}H, ^{13}C NMR, elemental analysis, electrospray ionisation mass spectrometry (ESI-MS), UV-visible (UV-vis) and infrared attenuated total reflection (IR-ATR) spectroscopy. The parent peak in ESI-MS was due to the species $[M+H]^+$; small amounts of $[M+Na]^+$ were also present. In the Supporting, the ESI-MS spectrum of **L1** (Fig. S1) is reported. In the IR spectra, the stretching of the carbonyl group was the principal signal, falling in the range 1717 – 1731 cm^{-1}, depending on the ligand. The IR spectra are reported in the Supporting Information (Fig. S2A-S7A). In the electronic spectra of coumarins, the absorptivity of the ligands varies in the 2500 – 16000 L mol^{-1} cm^{-1} range. All the ligands show a narrow band at ≈ 225 nm and a broad band at ≈ 300 nm with shoulders at higher and lower wavelengths. At ≈ 300 nm the absorptivity is in the order **L1** > **L4** > **L2** > **L6** ≡ **L3** > **L5**, while at ≈ 225 nm the order is **L4** > **L1** > **L2** >**L5** > **L6** > **L3**.

2.1.1 Crystal structure of coumarins

Crystals of **L4** and **L6** suitable for X-ray structure determination were obtained. From the attempt to crystallize **C1**, crystals of the **L1**·$HClO_4$ compound were obtained. A summary of the crystal data and structure determination procedures is reported in Table 1. In **L4** and **L6** four molecules are located in the crystallographic cells, the cumarinic rings of two molecules are parallel in pairs and the relative planes are tilted by 128.00° and 148.98°, respectively. No hydrogen bonds are formed. The pyridinic rings of the molecules are located in four distinct planes but almost parallel (max 1.96°, distance 2.265 Angstrom) in L4 and parallel two by two in L6 (distances 5.375 and 5.183 Angstrom, 36.45°). In compound **L1**·$HClO_4$, we observe a conformation different from those observed in **L4** and **L6**, due to the pyridinic ring N-H···O5 intramolecular hydrogen bond and the N-H···O1 intermolecular one with the perchlorate ion. The four ligand molecules lie in planes tilted by

0.00, 2.80 and 4.29 degrees and the pyridinic rings are located in four distinct planes, parallel two by two as in L6 (distances 4.567 and 6.787 Angstrom, 47.92°). ORTEP diagrams together with two packing views for **L1**·$HClO_4$, **L4**, and **L6** are shown in Figs. 2A, 2B, and 2C, respectively.

X-ray crystallographic data in CIF format have been deposited with the Cambridge Crystallographic Data Centre, CCDC no. 1561590-1561592.

2.2. Synthesis and characterization of copper complexes

By reacting ligands and copper(II) perchlorate in a 2:1 ligand:metal molar ratio in aqueous solution, green-brown complexes with general formula $CuL_2(H_2O)(ClO_4)_2$ (**C1-C6** for L = **L1-L6**) were obtained. The stoichiometry of the complexes was proposed on the basis of the elemental analysis. The synthesized complexes were air stable, fully soluble in CH_3CN and DMSO, and slightly soluble in water (at μM concentration). Complexes were characterized by elemental analysis, ESI-MS, UV-vis and IR-ATR spectroscopy. In the IR-ATR spectra, the characteristic peaks of the ClO_4^- anion and coordinated carbonyl groups were present. The IR spectra are reported in the Supporting Information (Fig. S2B-S7B). In the ESI-MS spectra, the peak of the species $[CuL_2(ClO_4)]^+$ was found for all of the systems. The peak of $[Cu^IL_2]^+$ was also observed, due to the reduction of Cu(II) to Cu(I), common in the ESI phase for acetonitrile solution of copper(II) complexes [34]. The ESI-MS spectra of **C1** is reported in the Supporting Information (Fig. S8) as an example. The UV-Vis spectra of the Cu(II) complexes were recorded in PIPES buffer solution (0.02 M) at pH 7.0 to increase their water solubility. In the absorption spectra of the complexes, the same bands of the ligands are present, but with absorptivity 2-4 times higher.

Since any attempt to obtain crystals suitable for X-ray analysis was unsuccessful, the coordination mode around the metal ion as isolated cationic species $[CuL_2(H_2O)]^{2+}$ was assessed on the basis of spectroscopic results and theoretical calculations. A trigonal bypiramidal geometry was obtained as the most stable structure. The likely structure of the Cu(II) complexes **C2** is shown in Fig. 3 as an

example. In the equatorial plane, the oxygen atoms of the carbonyl groups and water molecule are located, while the axial positions are occupied by the nitrogen atoms of the pyridine rings. The two ligands are arranged so as to minimize the steric hindrance.

2.3 DNA binding

Electronic absorption spectroscopy was employed to study the binding mode of the synthesized ligands and complexes with DNA. All the ligands and the corresponding complexes were able to interact with DNA, with binding constants ranging from 1.4 x 10^4 to 5.01 x 10^8 M^{-1} (see Table 3). Selected spectra recorded during the UV-Vis titrations of **L4**, **L2** and their metal complexes with DNA are reported in Fig. 4 as an example. With increasing DNA concentration, the absorption bands of ligands and complexes showed decreases in molar absorptivity (hypochromism) while a wide band was formed at ≈ 260 nm (where DNA also absorbs). The presence of isosbestic points in all the systems indicated the presence of two or more species in equilibrium. The number of linearly independent absorbing species was obtained by linearization of the absorbance data matrix [37]. Three eigenvalues were obtained for all the systems, corresponding to the three species free ligand, free DNA and the adduct Ligand-DNA (L-DNA). The DNA-binding constants (Table 2) were obtained by using the Hyperquad 2006 program [38] . The DNA binding constants were in the order **L3** > **L4** > **L1** > **L6** > **L5** > **L2** for ligands and in the order **C5 > C1 > C4 > C3 >> C2 ≈ C6** for the complexes. As regards the ligands, the presence of chlorine and fluorine as substituents weaken the interaction of the pyrido-coumarin moiety with DNA. On the other hand, the methoxy group enhanced this interaction, in particular when present in the 6th position of the aromatic ring. As regards the copper complexes, the presence of chlorine leads to the highest interaction with DNA, while fluorine substituents weaken such interaction (10^5 *vs* 10^3).

The logarithm of the ratio of substituted and unsubstituted ligand binding constants can be correlated with the Hammett σ parameter which accounts for the resonance and inductive effects of the substituent in the benzene ring; the σ parameters are tabulated [39,40]. A linear trend was

observed considering the derivatives with substituents in position 6 and 7, and the correlation was greater for the molecules with a substituent in 6 (Fig. 5).

Substituents in the 6 and 7 positions are in the *para* and *meta* positions with respect to the carbon atom 4a implicated in the carbonyl group. The linear trends evidenced in Fig. 5 suggest that the interaction between the coumarins and the DNA actually involves the carbonyl group. This hypothesis is supported by experimental evidence. In fact, the copper complexes, in which the carbonyl group is involved in the metal coordination, interact with DNA to a lesser extent, and this phenomenon is more relevant when the substituent is a methoxyl group. The experimental evidence suggests that the substituents show a limited direct interaction with DNA *via* a hydrogen bond.

2.4 Molecular docking

To clarify the interaction and binding affinity between the ligands and complexes with DNA, docking studies were performed on B-DNA (PDB ID: 1BNA) in presence of ligands or complexes. In Fig. 6 the docked **L3**-DNA, **L4**-DNA, **C3**-DNA and **C4**-DNA systems are shown, respectively. As shown by the docking studies, the ligands interact with DNA to a greater extent with respect to the copper complexes, confirming the binding constants experimentally determined.The ligands are able to enter the DNA grooves and form hydrogen bonds with carbonyl or lactonic oxygen, while the corresponding complexes show only Van der Waals interactions and a weak pi-pi stacking with the DNA basis rings. The lower interaction with DNA shown by the complexes is probably due to their steric hindrance that prevents the formation of hydrogen bonds with the carbonyl group.

The resulting minimum relative binding energy of the docked coumarin compounds **L3**- and **L4**-DNA was found to be -7.8 -7.7 kcal mol^{-1}. In the case of L3, which shows the highest DNA binding constant, two hydrogen bonds between *i*) the carbonyl oxygen and the DG10-NH2 protons (2.09 Angstrom) and *ii*) the lactonic oxygen and the DG10-NH2 protons (2.08 Angstrom) are present, with bond angles O—H--O of 141° and 132° respectively. In both cases, the proton is oriented

towards the heteroatom lone pairs. **L4** interacts with DG10-NH2 and shows similar distances and angles bonding to the **L3**-DNA complex.

2.5 QSAR descriptors

To rationalize the DNA binding constants shown by the series of ligands and copper complexes, some quantitative structure-activity relationship (QSAR) descriptors were calculated. The parameters considered were: polar surface area, hydrogen-bond acceptor, polar area, accessible polar area, polarizability, minimum value of the electrostatic potential (as mapped onto an electron density surface), maximum value of the electrostatic potential (as mapped onto an electron density surface), energy band gap, electronegativity, hardness, global softness, chemical potential, global electrophilicity index, and dipole moment (Table 4). In the case of ligands, a linear correlation was found between the log of K binding and the energy of the highest occupied molecular orbital (HOMO) or with the dipole moments, while no correlation was found for the complexes (Fig. 7). The calculated parameters were tentatively correlated also with the antiproliferative activity but no trend was observed for ligands or complexes. This suggests that the cytotoxic activity of the coumarin derivatives studied in this work is exerted on targets different from the DNA.

2.6 Antiproliferative activity

The antiproliferative activity of the ligands and complexes was tested against a series of human derived tumoral cell lines and against one healthy cell line. The IC_{50}, i.e. the concentration required to inhibit the antiproliferative activity by 50%, are reported in Table 3.

The ligands are devoid of cytotoxic activity against the tumour cell lines DU-145, and practically, HEP-G2 and against the healthy cell line CRL 7065. Pyridine-coumarine **L1** and **L4** are devoid of cytotoxic activity against all the studied cell lines. The coumarin derivatives with fluorine, in particular **L2**, show toxicity against CCRF-SB and SK-MES. The ligand **L5** shows low activity only towards CCRF-CEM and CCRF-SB. The **L6** is active, even if only poorly, towards CCRF-SB.

The copper complexes are inactive against prostatic and practically also hepatic carcinoma, showing activity against the leukemic cell lines and lung carcinoma. The complexes are also toxic towards the healthy cell line, except for **C1** and **C5**. These two complexes might be used as antitumoral agents as they are active against tumoral cells and inactive against healthy cells. As regards the ligands, only **L2** shows moderate anti-tumoral activity and good selectivity. The other ligands, while not presenting activity versus tumoral cells, are inactive also against the normal cells; being fluorescent, they might find applications as sensors in biomedical fields, though this is outside the scope of this work.

Conclusion

Novel 3-(pyridin-2-yl)coumarins derived from substituted salicylaldehydes and 2-pyridylacetonitrile were prepared and characterized. Complexes with copper(II) were prepared and the study was extended to three other similar coumarins. The cytotoxic activities of the ligands and complexes were studied against a series of human derived tumoral cell lines and one normal cell line. Ligand **L6** was active against leukemic cells and lung carcinoma and devoid of activity against normal cells. The other ligands presented in general low activities. The copper complexes were moderately active against the tested tumoral cell lines. In particular, **L3** was active against leukemia cells and lung carcinoma and was devoid of cytotoxic activities against normal cells. The IC_{50} values of the copper complexes were comparable with those reported in the literature for similar compounds. The ligands and complexes were able to interact with DNA and the interaction was greater for the former. This interaction involves the carbonyl group of the coumarin moiety, as evidenced by the molecular docking and Hammet correlation. QSAR studies show that the DNA binding constants were related to the molecular orbitals of the ligands, however no specific trend was observable between the DNA binding constants and the IC_{50}, suggesting that the biological activity of the studied molecules is exerted by mechanisms other than the DNA interaction.

The linear correlation between the logarithm of the binding constants and the HOMO energy shows that the interaction with DNA depends on the nucleophilicity of the coumarins. In this kind of interaction, covalent bonds are not formed, and therefore, it is the formation of hydrogen bonds that drives the DNA binding.

3. Experimental part

3.1 Materials and methods

Ethanol, methanol, perchloric acid, chloridric acid, anhydrous ethanol, calf-thymus DNA (ct-DNA), piperazine-1,4-bis(2-ethanosulfonic) acid (PIPES) and piperidine were purchased from Aldrich (Milan, Italy). Salicylicaldehyde, salicylic aldehyde derivatives, and pyridine acetonitrile were purchased from Alfa-Aesar. The commercial reagents were used as received, without any further purification. Ultra-pure water obtained with MilliQ Millipore was used for mass spectrometry and DNA interaction studies. Melting points were obtained on a Kofler hot stage microscope and are uncorrected. NMR spectra were recorded in $CDCl_3$ on a 400 Varian spectrometer at room temperature with TMS as an internal standard. Chemical shifts, multiplicity and coupling constants were all reported. Mass spectra were recorded on a triple quadruple QqQ Varian 310-MS mass spectrometer using electrospray ionisation (ESI) technique. The mass spectra were recorded in positive ion mode in the *m/z* 50–1000 range. The experimental conditions were: needle voltage 4500 V, shield voltage 800 V, housing temperature 60 °C, drying gas temperature 150 °C, nebuliser gas pressure 40 PSI, drying gas pressure 40 PSI, and detector voltage 1650 V. Tandem MS–MS experiments were performed with argon as the collision gas (1.8 PSI) using a needle voltage of 6000 V, shield voltage of 800 V, housing temperature of 60 °C, drying gas temperature of 150 °C, nebuliser gas pressure of 40 PSI, drying gas pressure of 40 PSI, and a detector voltage of 2000 V. The isotopic patterns of the measured peaks in the mass spectra were analysed using the mMass 5.5.0 software package [41,42]. The assignments were based on the copper-63 isotope. The sample

solutions were infused directly into the ESI source using a programmable syringe pump at a flow rate of 1.0 mL/h. A dwell time of 14 s was used and the spectra were accumulated for approx. 5 min in order to increase the signal-to-noise ratio.

General procedure for the preparation of chromen-2-one derivatives.

Salicylaldehyde derivatives (0.0082 mol) and pyridine-2-acetonitrile (0.94 mL, 0.0082 mol) were dissolved in 15 mL of anhydrous ethanol and cooled at 0 °C with an ice bath. Piperidine (0.3 mL) was then added stepwise. The mixture was stirred for 20 h at room temperature, then treated with HCl (50 mL, 3.5%) and refluxed for 10 h to hydrolyse the iminocoumarins. When the reaction was finished, the acidic solution was basified with aqueous ammonia. The precipitate was filtered and recrystallized from methanol to yield the desired product [36].

3-(pyridin-2-yl)-2H-chromen-2-one (L1).

Yield: 87%, mp 142-144 °C. Experimental data are consistent with those reported in the literature [36]. IR-ATR (cm^{-1}): 1718 (C=O); ESI-MS (Calcd and found, *m/z*): 224.07 [L + H]; UV-Vis ε_{302nm} = 12354 cm mol^{-1} L^{-1} (PIPES 0.02M pH 7.0).

6-fluoro-3-(pyridin-2-yl)-2H-chromen-2-one (L2)

Yield: 71%, mp 191 °C; ^{1}H NMR (400 MHz, $CDCl_3$, δ, ppm): 7.26-7.38 (m, 4H), 7.80 (dt, 1H, J = 7.8 Hz, J = 1.8 Hz), 8.42 (d, 1H, J = 8.1 Hz), 8.69 (d, 1H, J = 4,7 Hz), 8.72 (s, 1H); ^{13}C NMR (101 MHz, CDCl3, δ, ppm): 113.6 (d, JCF = 24.2 Hz), 117.8 (d, JCF = 8.1 Hz), 119.4 (d, JCF = 25.3 Hz), 120.1 (d, JCF = 9.1 Hz), 123.7, 124.0, 126.3, 136.6, 141.2 (d, JCF = 3.0 Hz), 149.4, 150.0, 150.7, 158.6 (d, JCF = 245.4 Hz), 159.8; IR-ATR (cm^{-1}): 1718 (C=O); ESI-MS (Calcd, found, *m/z*): 242.06, 242.02 $[L + H]^+$; UV-Vis ε_{272nm} = 8007 cm mol^{-1} L^{-1} (PIPES 0.02 M pH 7.0).

7-methoxy-3-(pyridin-2-yl)-2H-chromen-2-one (L3)

Yield: 54%, mp 144 °C; ^{1}H NMR (400 MHz, $CDCl_3$, δ, ppm): 3.90, (s, 3H), 6.87-6.90 (m, 2H), 7.25-7.28 (m, 1H), 7,54 (d, 1H, J = 8.4 Hz), 7.77 (br.t, 1H, J = 7.8 Hz), 7.40 (d, 1H, J = 8.1 Hz),

8.66 (d, 1H, J = 4.7 Hz), 8.73 (s, 1H); ^{13}C NMR (400 MHz, $CDCl_3$, δ, ppm): 55.79, 100.20, 113.06, 113.24, 121.80, 122.94, 123.42, 129.84, 136.55, 142.54, 149.23, 151.65, 155.83, 160.57, 163.27; IR-ATR (cm^{-1}): 1734(C=O); ESI-MS (Calcd and found, *m/z*): 254.08 $[L + H]^+$; UV-Vis ε_{342nm} = 2673 cm mol^{-1} L^{-1} (PIPES 0.02 M pH 7.0).

6-methoxy-3-(pyridin-2-yl)-2H-chromen-2-one (L4)

Yield: 76%, mp 166-167 °C; ^{1}H NMR (500 MHz, $CDCl_3$, δ, ppm): 3.84 (s, 3H, OCH_3), 7.04 (d, 1H, *J* = 3 Hz), 7.13 (dd, 1H, *J* = 9.0 Hz, *J* = 2.5 Hz), 7.27-7.30 (m, 2H), 7.77 (bt, 1H, *J* = 7.5 Hz), 8.42 (d, 1H, *J* = 7.5 Hz), 8.67 (d, 1H, *J* = 7.5 Hz), 8.71 (s, 1H); ^{13}C NMR (400 MHz, $CDCl_3$, δ, ppm): 56.00, 110.62, 117.55, 120.03, 120.37, 123.61, 124.25, 125.79, 136.81, 142.47, 148.64, 149.55, 151.54, 156.35, 160.61; IR-ATR (cm^{-1}): 1731 (C=O); ESI-MS (Calcd, found, *m/z*): 254.08, 254.09 $[L + H]^+$; UV-Vis ε_{293nm} = 10560 cm mol^{-1} L^{-1} (PIPES 0.02 M pH 7.0).

6-chloro-3-(pyridin-2-yl)-2H-chromen-2-one (L5).

Yield: 76%, mp 170 °C; ^{1}H NMR data are consistent with those reported in the literature [43]; ^{13}C NMR (400 MHz, $CDCl_3$, δ, ppm): 117.73, 120.47, 123.70, 124.04, 126.34, 127.79, 129.77, 131.92, 136.63, 140.94, 149.42, 150.67, 152.15, 159.57; IR-ATR (cm^{-1}): 1717 (C=O); ESI-MS (Calcd and found, *m/z*): 258.03 $[L + H]^+$; UV-Vis ε_{294nm} = 2349 cm mol^{-1} L^{-1} (PIPES 0.02 M pH 7.0).

7-fluoro-3-(pyridin-2-yl)-2H-chromen-2-one (L6)

Yield: 77%, mp. 159-161 °C; ^{1}H NMR (500 MHz, $CDCl_3$, δ, ppm): 7.02-7.10 (m, 2H), 7.29 (dd, 1H, J =7.5 Hz, J =4.7 Hz), 7,62 (dd, 1H, J = 8.4 Hz, J = 6.1 Hz), 7.77 (t, 1H, J = 7.8 Hz), 8.38 (d, 1H, J = 8 Hz), 8,66 (d, 1H, J = 4.7 Hz), 8.74 (s, 1H); ^{13}C NMR (101 MHz, $CDCl_3$, δ, ppm): 103.9 (d, JCF = 25.7 Hz), 112.8 (d, JCF = 23.1 Hz), 116.2, 123.4, 123.8, 124.0, 130.4 (d, JCF = 10.4 Hz), 136.6, 141.7, 149.3, 150.9, 154.9 (d, JCF = 13.0 Hz), 169.7, 164.7 (d, JCF = 254.7 Hz); IR-ATR (cm^{-1}): 1723 (C=O); UV-Vis ε_{326nm} = 2770 cm mol^{-1} L^{-1} (PIPES 0.02 M pH 7.0).

3.2 Synthesis of copper complexes $CuL_2(H_2O)(ClO_4)_2$ (C1-C6)

To an ethanolic solution of the ligand (0.1 g, 5 mL) an ethanolic solution of $Cu(ClO_4)_2$ (1:2 copper:ligand molar ratio) was added drop by drop. A solid product was formed. The mixture was stirred for ten minutes, and the product was filtered, washed with water and dried at room temperature. The obtained compounds were re-crystallised from methanol as microcrystalline powder. The compounds were characterized by elemental analysis, mass spectrometry and IR-ATR. Analytical results: **C1** $CuC_{28}H_{20}N_2O_{13}Cl_2$ calc. C 46.35%, H 2.78%, N 3.86%, found C 46.18%, H 2.79%, N 3.85%; **C2** $CuC_{28}H_{18}N_2O_{13}F_2Cl_2$ calc. C 44.16%, H 2.38%, N 3.68%, found C 44.10%, H 2.37%, N 3.67%; **C3** $CuC_{30}H_{24}N_2O_{15}Cl_2$ calc. C 45.86%, H 3.08%, N 3.57%, found C 45.82%, H 3.07%, N 3.58%; **C4**: $CuC_{30}H_{24}N_2O_{15}Cl_2$ calc. C 45.86%, H 3.08%, N 3.57%, found C 45.88%, H 3.09%, N 3.56%; **C5** $CuC_{28}H_{18}N_2O_{13}Cl_4$ calc. C 42.38%, H 2.29%, N 3.53%, found C 42.42%, H 2.30%, N 3.52%; **C6** $CuC_{28}H_{18}N_2O_{13}F_2Cl_2$ calc. C 44.16%, H 2.38%, N 3.68%, found C 44.05%, H 2.37%, N 3.69%;. ESI-MS $[M\text{-}H_2O\text{-}ClO_4]^+$ **C1** calc. *m/z* 607.96, found *m/z* 608.12, **C2** *m/z* calc. 643.44 found m/z 644.17, C3 calc. m/z 667.96, found *m/z* 668.11, **C4** calc. *m/z* 667.96, found *m/z* 668.31, **C5** calc. *m/z* 675.87, found *m/z* 676.01, **C6** calc. m/z 673.92, found m/z 673.85. UV-Vis: **C1** ε_{306nm} = 20964 cm mol^{-1} L^{-1}, **C2** ε_{294nm} = 23534 cm mol^{-1} L^{-1}, **C3** ε_{338nm} = 23305 cm mol^{-1} L^{-1}, **C4** ε_{296nm} = 33448 cm mol^{-1} L^{-1}, **C5** ε_{268nm} = 16263 cm mol^{-1} L^{-1}, **C6** ε_{366nm} = 8868 cm mol^{-1} L^{-1} (PIPES 0.02 M pH 7.0).

3.3 DNA INTERACTION

The binding constants (Kb) between ct-DNA and the coumarin ligands or copper-coumarin complexes were determined at 25 °C by spectrophotometric titrations in PIPES buffer 0.02 M at pH 7.0. The UV–vis measurements were carried out on an Agilent Cary 60 spectrometer (1 cm path length). The stock solution of ct-DNA in 0.02 M PIPES buffer at pH 7.0 was stored at 4 °C and used within four days. The concentration of DNA per nucleotide was determined by UV absorption at 260 nm using its molar absorption coefficient (6600 M^{-1} cm^{-1}) [44]. The purity of the DNA was

checked by monitoring the ratio of the absorbance at 260 nm to that at 280 nm. A ratio higher than 1.8 indicated a DNA sufficiently protein free [45]. Thirty solutions containing a fixed amount of ligand or metal complex (ranging from ≈ 2.0 x 10^{-5} to ≈ 5.2 x 10^{-5} mmol, according to compound absorptivity) and variable amounts of DNA (ranging from 0 to 2.6 x 10^{-4} mmol) were prepared and stored in the dark at room temperature for 24 h before the absorbance measurements. Absorption spectra were recorded in the 200–500 nm range. The necessary delay time for reaching the equilibrium was assessed spectrophotometrically by determining the time after which changes in UV–vis spectra were not observed (≈20 h).

3.4 Theoretical calculations

Molecular docking studies on ligands and complexes were carried out using Vina Autodock [46] and Python Molecular Viewer (PMV) [47]. Ligand and complex geometries were optimised with SPARTAN'14 (Wavefunction Inc.) by using the density functional theory at the B3LYP level (6-31G* basis sets). The optimized molecules were exported as a pdb file and used with PMV. The structure of B-DNA (PDB ID: 1BNA) was retrieved from the protein data bank (http://www.rcsb.org./pdb) and pre-treated with PMV [48]. The docked molecules were visualized with PMV. QSAR descriptors were obtained with SPARTAN'14 (Wavefunction Inc.) by using the density functional theory at the B3LYP level (6-31G* basis sets).

3.5 Cell cultures

In this study, the following human hematologic and solid tumour-derived cell lines were used: acute T-lymphoblastic leukaemia (CCRF-CEM), acute B-lymphoblastic leukaemia (CCRF-SB), lung squamous carcinoma (SK-MES-1), prostate carcinoma (DU-145), and hepatocellular carcinoma (Hep-G2). The human foreskin cell line (CRL 7065) was used as a control of normal cells to determine the degree of selectivity of test compounds towards cancer cells.

All cell lines were purchased from the American Type Culture Collection (ATCC, USA) and were

cultured in their specific conditions and media according to ATCC instructions (37 °C, 5% CO2, with 5– 10% foetal bovine serum, antibiotic, and sodium pyruvate unless otherwise indicated). All cell lines were maintained in exponential growth by periodically splitting high density suspension cultures (i.e. 10^6/mL) of hematologic tumour-derived cell lines, or when solid tumour-derived cell monolayers reached sub-confluence (70–90% confluence). Cell cultures were periodically tested for the absence of mycoplasma with an N-GARDE Mycoplasma PCR Reagent kit (Euroclone).

3.6 Antiproliferative activity

The antiproliferative activity of compounds was evaluated against hematologic and solid tumour-derived cells in exponentially growing cell cultures. Adherent cells were seeded at a density of 5 × 10^4 cells/mL in each well of 96-well flat bottomed plates. Cell cultures were incubated overnight before the addition of 2 × the final concentrations of test compounds (four replicates/concentration). Cell suspensions of non-adherent cells were seeded at a density of 1 × 10^5 cells/mL per well of 96-well flat bottomed plates, and treated with 2× the final concentrations of each compound (four replicates/concentration). Cell viability was determined after 96 h of incubation at 37 °C, 5% CO2, by the 3-(4,5-dimethyl- thiazol-2-yl)-2,5-diphenyl-tetrazolium bromide (MTT) method [49]. Dose–response curves and compound concentrations, required to reduce the cell proliferation by 50% (IC_{50}) compared to untreated controls, were determined for each compound by non-linear curve fitting. All data reported represent the mean values ± SD of three to four independent experiments.

Table of Abbreviations

CCRF-Cem human acute T-lymphoblastic leukaemia; CCRF-Sb human acute B-lymphoblastic leukaemia; Sk-Mes-1 human lung carcinoma; Du 145 human prostate carcinoma; Hep-G2 human hepatocellular carcinoma; CRL 7065 human normal foresti; QSAR quantitative structure-activity relationship; ESI-MS electrospray ionisation mass spectrometry; IR-ATR infrared attenuated total

reflection spectroscopy; PIPES piperazine-1,4-bis(2-ethanosulfonic) acid ; DMSO dimethylsulphoxide; HOMO highest occupied molecular orbital; ct-DNA calf-thymus.

Bibliographic References

[1] J. Klenkar, M. Molnar, J. Chem. Pharm. Res. 7 (2015) 1223–1238.

[2] K.N. Venugopala, V. Rashmi, B. Odhav, Biomed Res. Int. 2013 (2013) 1–14.

[3] K. Rohini, S. PS, J. of Thermodynamics & Catalysis, 5 (2014) 5–7. .

[4] H. Xiongfeng, L. Lvye, X. Qun, J. Rohrer, Determination of Coumarins in Cosmetics, Application Note 1128, Thermo Fisher Scientific

[5] J. Li, C.-F. Zhang, S.-H. Yang, W.-C. Yang, G.-F. Yang, Anal. Chem. 86 (2014) 3037–3042.

[6] E. Guardado Yordi, M.J. Matos, A. Pérez-Martínez, C. Tornes, L. Santana, E. Molina Pérez, E. Uriarte, Food Funct. (2017).

[7] P.K. Jain, H. Joshi, J. Appl. Pharm. Sci. 2 (2012) 236–240.

[8] Y. Bansal, P. Sethi, G. Bansal, Med. Chem. Res. 22 (2013) 3049–3060.

[9] D. Viña, M.J. Matos, M. Yáñez, L. Santana, E. Uriarte, Med. Chem. Commun. 3 (2012) 213–218.

[10] A. Basile, S. Sorbo, V. Spadaro, M. Bruno, A. Maggio, N. Faraone, S. Rosselli, Molecules. 14 (2009) 939–952.

[11] S. Vazquez-Rodriguez, R. Figueroa-Guíñez, M.J. Matos, L. Santana, E. Uriarte, M. Lapier, J.D. Maya, C. Olea-Azar, Med. Chem. comm. 4 (2013) 993-1000.

[12] F. Golfakhrabadi, M. Abdollahi, M.R.S. Ardakani, S. Saeidnia, T. Akbarzadeh, A.N. Ahmadabadi, A. Ebrahimi, F. Yousefbeyk, A. Hassanzadeh, M. Khanavi, Pharm. Biol. 52 (2014) 1335–1340.

[13] R.K. Singh, T.S. Lange, K.K. Kim, L. Brard, Invest. New Drugs. 29 (2011) 63–72.

[14] X. Xu, Y. Zhang, D. Qu, T. Jiang, S. Li, J. Exp. Clin. Cancer Res. 30 (2011) 33.

[15] M.A. Musa, M.O. F. Khan, J.S. Cooperwood, Lett. Drug Des. Discov. 6 (2009) 133–138.

[16] M. Rajabi, Z. Hossaini, M.A. Khalilzadeh, S. Datta, M. Halder, S.A. Mousa, J. Photochem. Photobiol. B. 148 (2015) 66–72.

[17] C. Li, X. Han, H. Zhang, J. Wu, B. Li, Trop. J. Pharm. Res. 14 (2015) 611–617.

[18] A. Haghighitalab, M.M. Matin, A.R. Bahrami, M. Iranshahi, M. Saeinasab, F. Haghighi, Z. Naturforsch. 69 (2014) 99–109.

[19] S. Mirunalini, K. Deepalakshmi, J. Manimozhi, Aging Pathol. 4 (2014) 131–135.

[20] C. Zwergel, S. Valente, A. Salvato, Z. Xu, O. Talhi, A. Mai, A. Silva, L. Altucci, G. Kirsch, Med chem comm. 4 (2013) 1571–1579.

[21] R.B. Moffett, J Med Chem. 7 (1964) 446–449.

[22] A.K.P.& N.H.P. D I Brahmbhatt, Ankit R Kaneria, Indian J. Chem. 49B (2010) 971–977.

[23] D.I. Brahmbhatt, J.M. Gajera, V.P. Pandya, M.A. Patel, Indian J. of Chem. 46 (2007) 869–871.

[24] U.R.P. D I Brahmbhatt, Indian J. Chem. 42B (2003) 145–149.

[25] R. Kenchappa, Y.D. Bodke, A. Chandrashekar, S. Telkar, K.S. Manjunatha, M. Aruna Sindhe, Arab. J. Chem. 10 (2017) S1336–S1344.

[26] F. Trudu, F. Amato, P. Vaňhara, T. Pivetta, E.M. Peña-Méndez, J. Havel, J. Appl. Biomed. 13 (2015) 79–103.

[27] V.R. Kotte Shylaja, Vasam Srinivas, G.Srikanth, Int. J. Mod. Chem. Appl. Sci. 3 (2016) 301–305.

[28] M. Grazul, E. Budzisz, Coord. Chem. Rev. 253 (2009) 2588–2598.

[29] Q.W. Ang, W.U. Jin-cai, N.T. Ang, Structure. 58 (2010) 1003–1008.

[30] M. Rajeshirke, R. Shah, P. Yadav, N. V Purohit, Der Pharmacia Sinica 3 (2012) 239–248.

[31] J. Jumal, D.M. Ibrahim, F.W. Harun, Middle-East J. Sci. Res. 23 (2015) 2946–2951.

[32] T. Pivetta, M.D. Cannas, F. Demartin, C. Castellano, S. Vascellari, G. Verani, F. Isaia, J. Inorg. Biochem. 105 (2011) 329–338.

[33] T. Pivetta, F. Isaia, G. Verani, C. Cannas, L. Serra, C. Castellano, F. Demartin, F. Pilla, M. Manca, A. Pani, J. Inorg. Biochem. 114 (2012) 28–37.

[34] T. Pivetta, F. Trudu, E. Valletta, F. Isaia, C. Castellano, F. Demartin, R. Tuveri, S. Vascellari, A. Pani, J. Inorg. Biochem. 141 (2014) 103–113.

[35] T. Pivetta, F. Isaia, F. Trudu, A. Pani, M. Manca, Talanta. 115 (2013) 84–93.

[36] T. Yu, S. Yang, J. Meng, Y. Zhao, H. Zhang, D. Fan, X. Han, Z. Liu, Inorg. Chem. Commun. 14 (2011) 159–161.

[37] M. Meloun, J. Čapek, P. Mikšík, R.G. Brereton, Anal. Chim. Acta. 423 (2000) 51–68.

[38] P. Gans, A. Sabatini, A. Vacca, Talanta. (1996) 1739–1753.

[39] H.H. Jaffe, Chem. Rev. (1953) 191–261.

[40] J. March, Advanced Organic Chemistry, New York, 1992.

[41] M. Strohalm, D. Kavan, P. Nova, M. Volny, Anal. Chem. 82 (2010) 4648–4651.

[42] T.H.J. Niedermeyer, M. Strohalm, PLoS One. 7 (2012) e44913.

[43] O. V. Khilya, O. V. Shablykina, M. S. Frasinyuk, V. V. Ishchenko, V. P. Khilya, Chemistry of Natural Compounds 41 (2005) 428–431.

[44] M.E. Reichmann, S.A. Rice, C.A. Thomas, P. Doty, J. Am. Chem. Soc. 76 (1954) 3047–3053.

[45] J. Murmur, J. Mol. Biol. 3 (1961) 208–218.

[46] O. Trott, J.A. Olson, J. Comput. Chem. 31 (2009) 455–461.

[47] M.F. Sanner, J. Mol. Graph. Mod. 17 (1999) 57–61.

[48] E.F. Pettersen, T.D. Goddard, C.C. Huang, G.S. Couch, D.M. Greenblatt, E.C. Meng, T.E. Ferrin, J. Comput. Chem. 25 (2004) 1605–1612.

[49] R. Pauwels, J. Balzarini, M. Baba, R. Snoeck, D. Schols, P. Herdewijn, J. Desmyter, E. De Clercq, J. Virol. Methods. 20 (1988) 309–321.

Figure legends:

Fig. 1. Molecular structure and acronyms of the coumarins studied in this work. **L1** is 3-(pyridin-2-yl)-2*H*-chromen-2-one, **L2** is 6-fluoro-3-(pyridin-2-yl)-2*H*-chromen-2-one, **L3** is 7-methoxy-3-(pyridin-2-yl)-2H-chromen-2-one, **L4** is 6-methoxy-3-(pyridin-2-yl)-2H-chromen-2-one, **L5** is 6-chloro-3-(pyridin-2-yl)-2*H*-chromen-2-one, **L6** is 7-fluoro-3-(pyridin-2-yl)-2*H*-chromen-2-one.

Fig. 2. ORTEP drawing of **L1**·HClO4 (**A**), **L4** (**B**) and **L6** (**C**). Ellipsoids drawn at 50% probability.

Fig. 3. Hypothesized structure of **C2** $[CuL_2(OH_2)]^{2+}$ (DFT analysis, B3LYP theory level, 6-31 G* basis set).

Fig. 4. Selected spectra recorded during titration of (**A**) **L4** (5.2 x 10^{-5} mmol), (**B**) **L2** (4.2 x 10^{-5} mmol), (**C**) **C4** (3.3 x 10^{-5} mmol) and (**D**) **C2** (4.3 x 10^{-5} mmol), with DNA (4.22 x 10^{-4} M); PIPES 0.02 M, pH 7.0. Arrows indicate the absorbance changes due to DNA addition.

Fig. 5. Trend between the logarithm of the ratio of substituted (K_b^{sub}) and unsubstituted (K_b^{uns}) ligand's DNA binding constants and the Hammett σ parameter for derivatives with substituents in position 6 and 7 (**A**) or in position 6 (**B**) ($Y_A = 0.08 - 0.12X$, $R^2 = 0.8571$; $Y_B = 1.4 \cdot 10^{-4} - 0.11X$, $R^2 = 1.000$).**Fig. 6**. Molecular docked model of **L3** (A), **L4** (B), **C3** (C) and **C4** (**D**) with DNA (PDB ID: 1BNA).

Fig. 7. Correlation between the log of the binding constant and the energy of the highest occupied molecular orbital (HOMO) (A) and with the dipole moments (B) for the ligands **L1**-**L6** ($Y_A = 9.1X + 61.4$, $R^2 = 0.9162$; $Y_B = 0.82X - 0.62$, $R^2 = 0.8229$).

Scheme legend

Scheme 1. Synthesis of the studied coumarin derivatives (Y = H, 6-F, 7-F, 6-OCH_3, 7-OCH_3, 6-Cl).

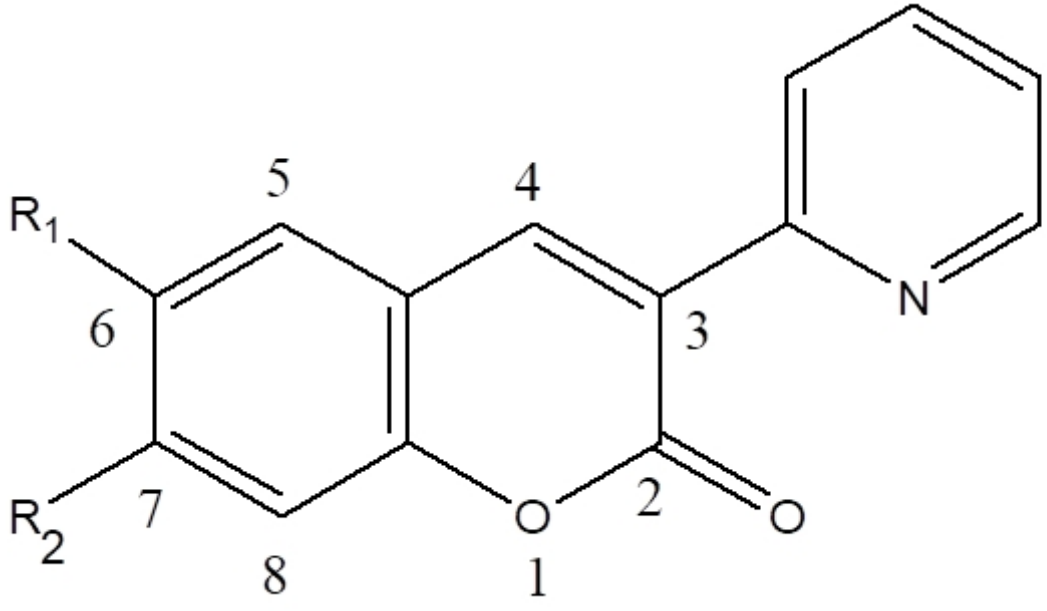

L1: $R_1 = R_2 = H$

L2 : $R_1 = F$, $R_2 = H$

L3 : $R_1 = H$, $R_2 = OCH_3$

L4 : $R_1 = OCH_3$, $R_2 = H$

L5 : $R_1 = Cl$, $R_2 = H$

L6 : $R_1 = H$, $R_2 = F$

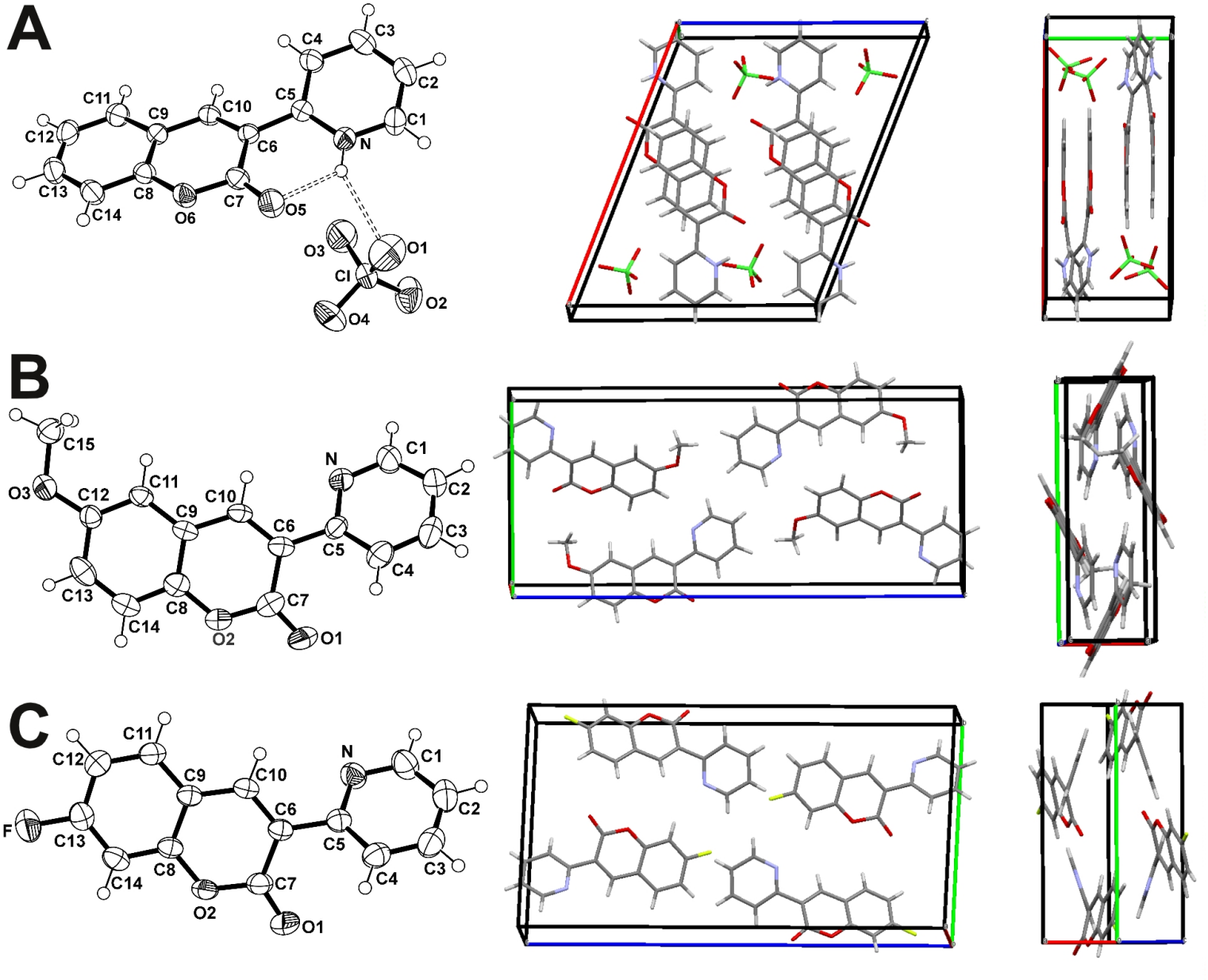
A
C4
C3
C2
C11
C9
C10
C5
C1
C12
C6
N
C13
C8
O6
C7
O5
C14
O3
O1
Cl
O2
O4
B
C15
N
C1
O3
C12
C11
C10
C9
C6
C2
C5
C3
C4
C13
C8
C7
C14
O2
O1
C
C11
C12
N
C1
C9
C10
C6
C2
F
C13
C5
C8
C4
C3
C14
C7
O2
O1

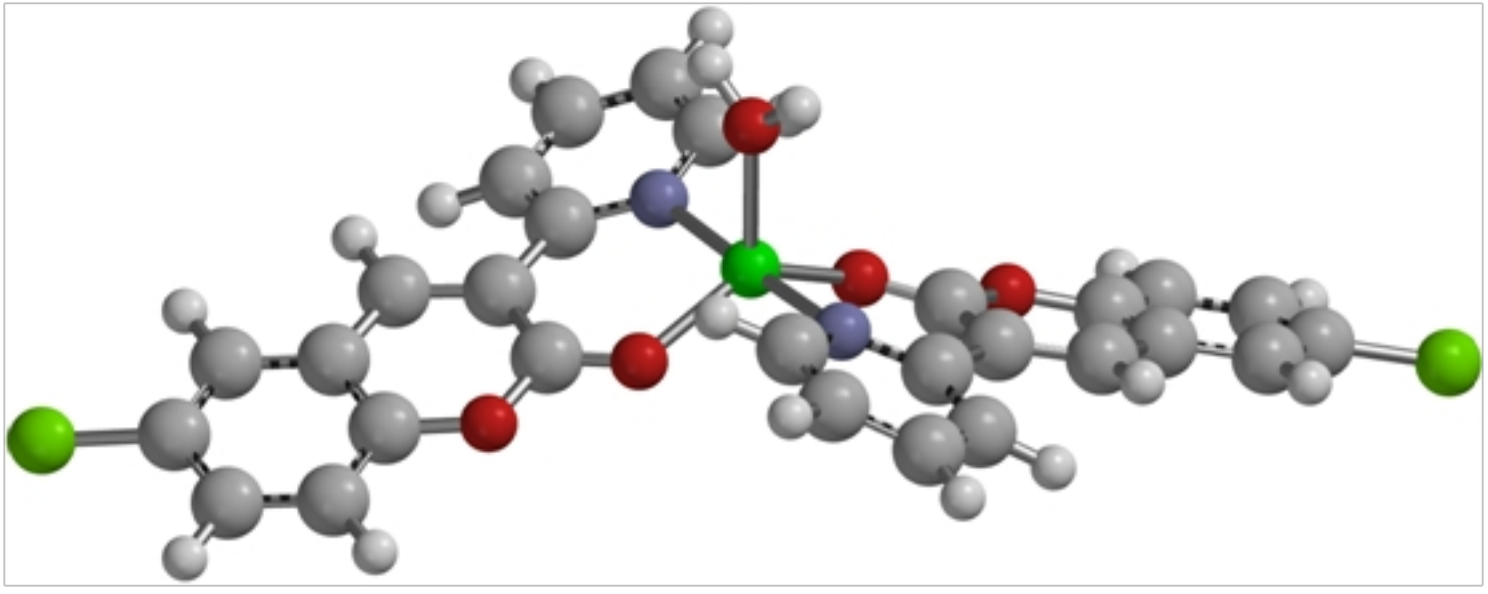

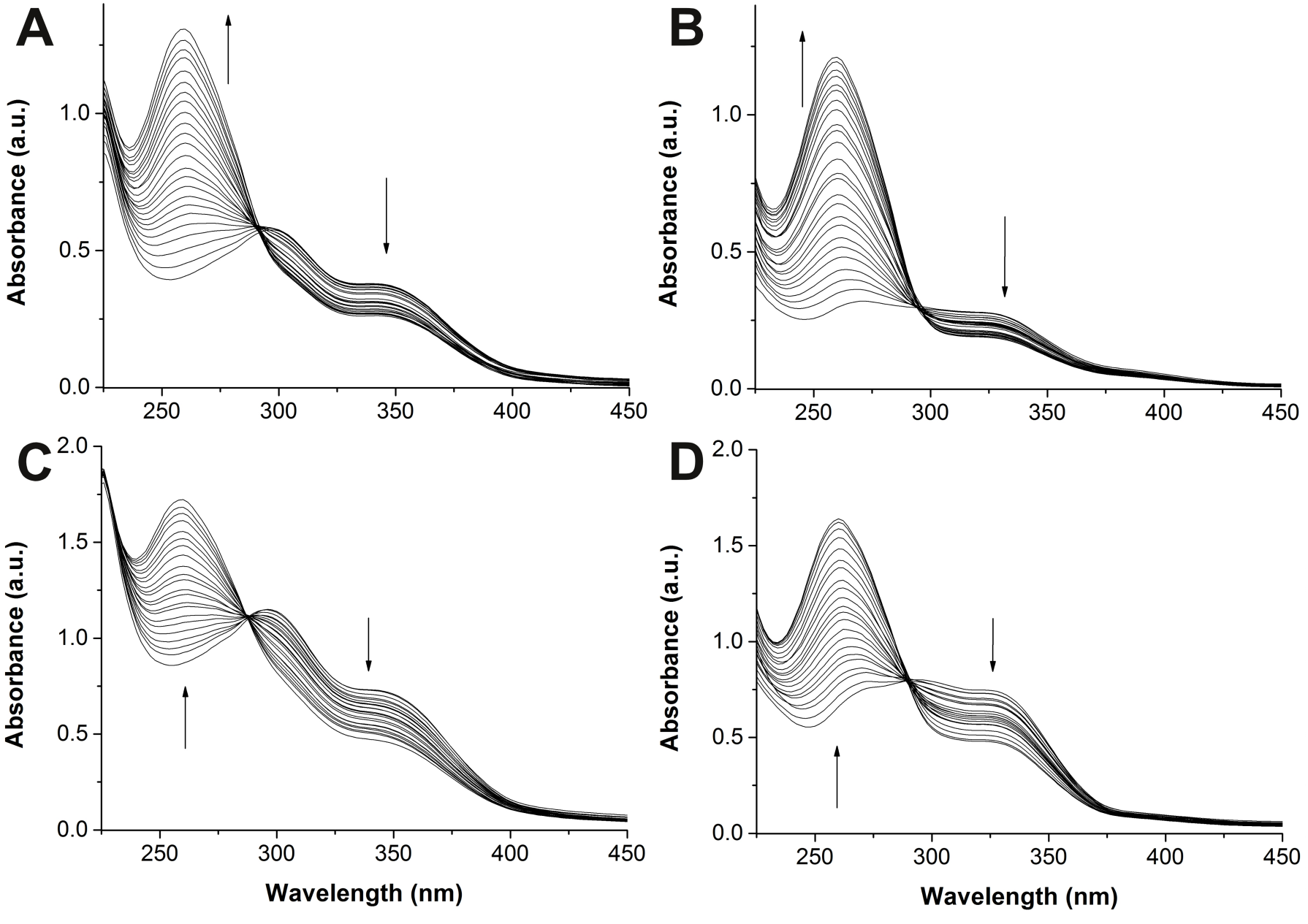
A
B
C
D
Absorbance (a.u.)
Wavelength (nm)
0.0
0.5
1.0
1.5
2.0
250
300
350
400
450

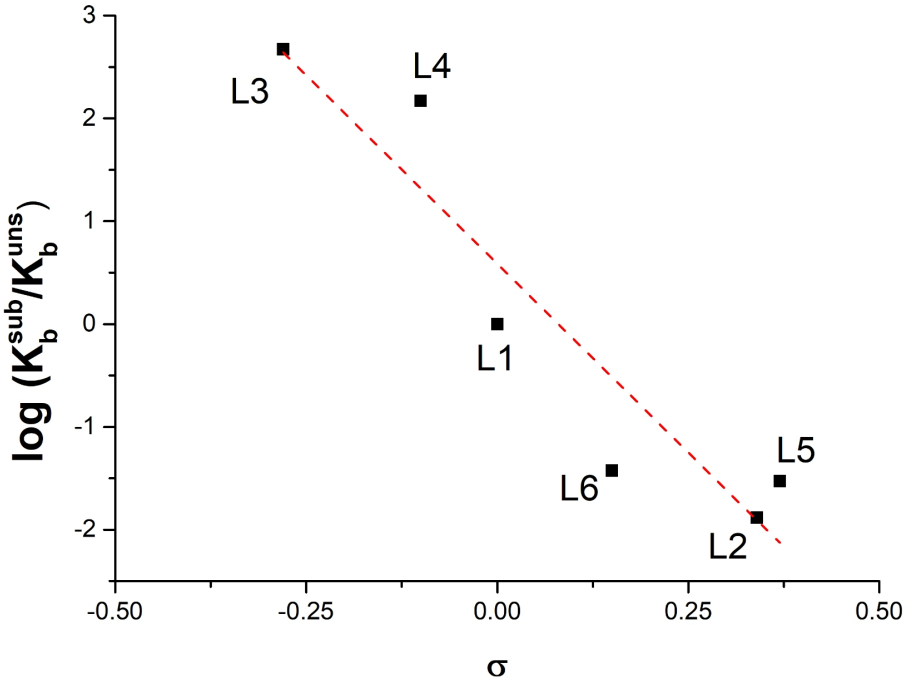
log (K_b^{sub}/K_b^{uns})
σ
L3
L4
L1
L6
L5
L2
3
2
1
0
-1
-2
-0.50
-0.25
0.00
0.25
0.50

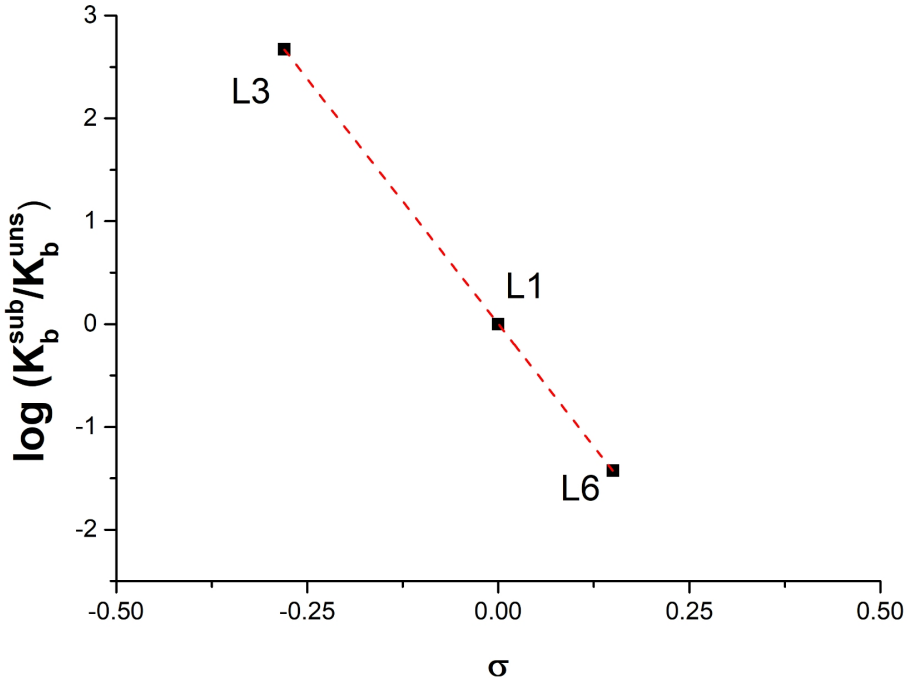
log (K_b^{sub}/K_b^{uns})
σ
L3
L1
L6
3
2
1
0
-1
-2
-0.50
-0.25
0.00
0.25
0.50

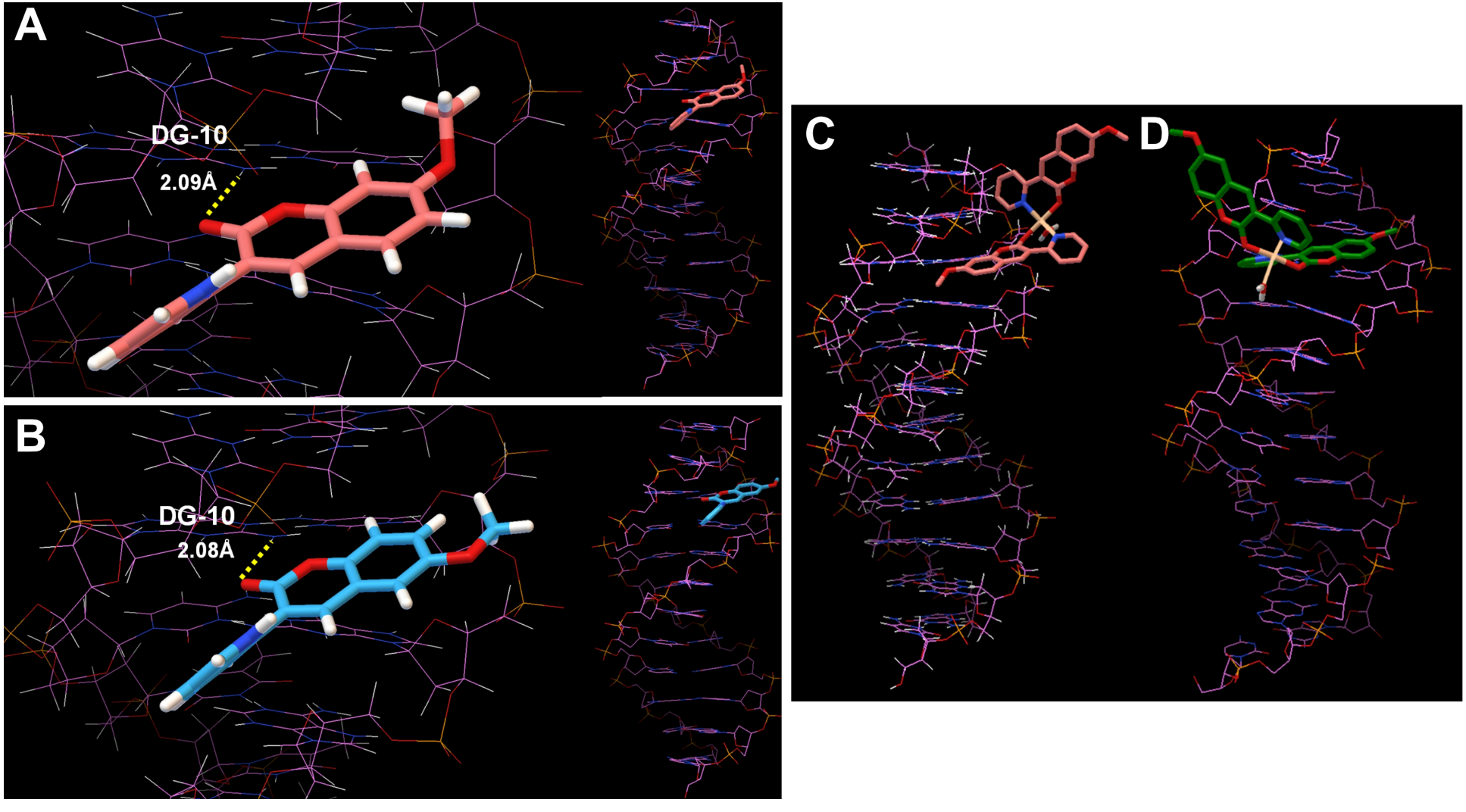
A
DG-10
2.09Å
B
DG-10
2.08Å
C
D

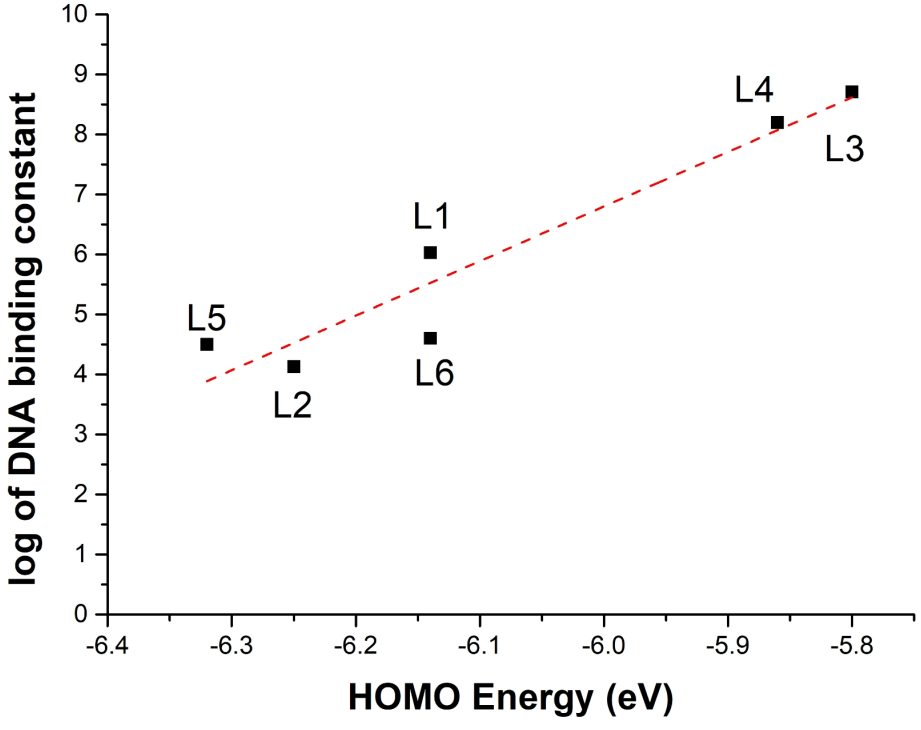
log of DNA binding constant
HOMO Energy (eV)
L1
L2
L3
L4
L5
L6

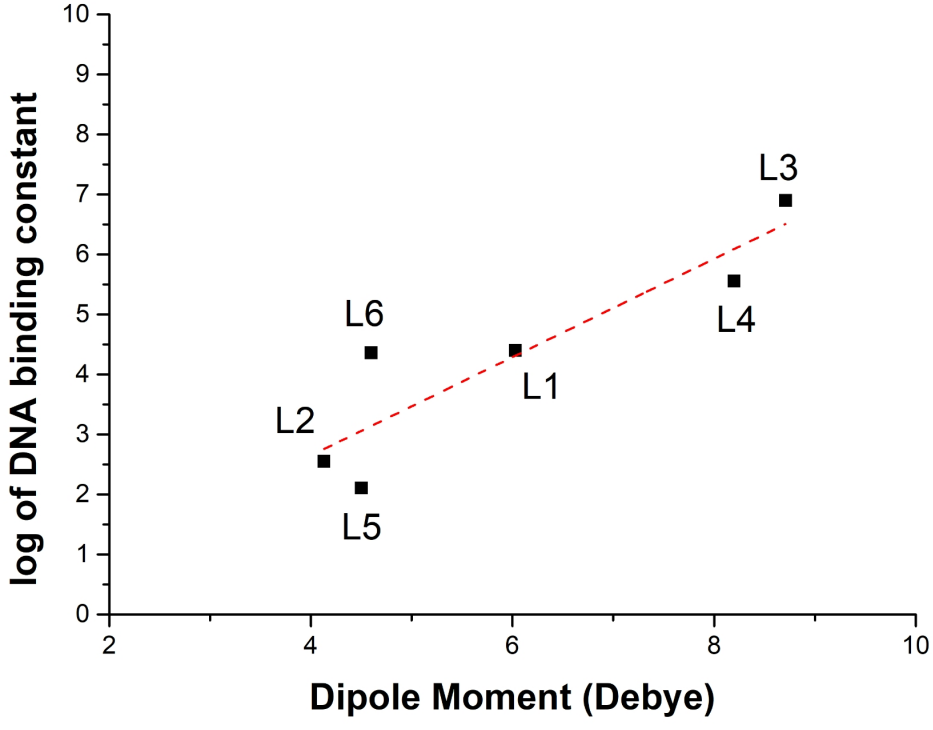
log of DNA binding constant
Dipole Moment (Debye)
L1
L2
L3
L4
L5
L6

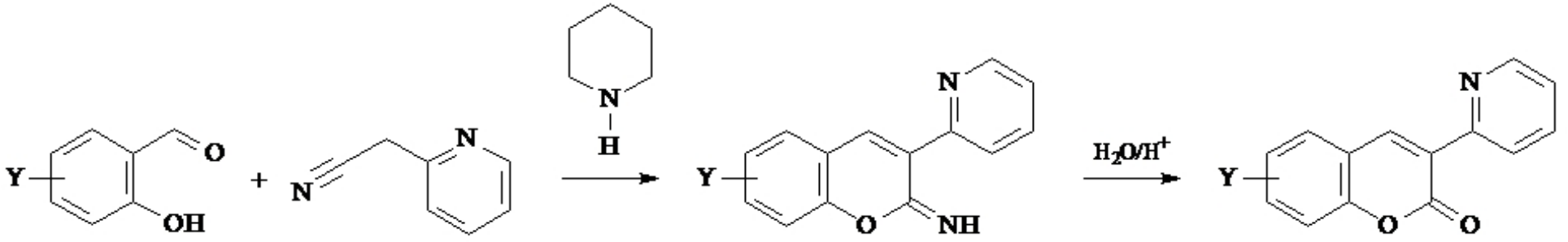

L1-6

Table 1. Crystallographic data and structure refinement details

Compound	**L1·HClO$_4$(1)**	**L4(2)**	**L6(3)**
Formula	$C_{14}H_{10}ClNO_6$	$C_{15}H_{11}NO_3$	$C_{14}H_8FNO_2$
Crystal system	monoclinic	monoclinic	monoclinic
Space group	$P2_1/c$ (no. 14)	$P2_1/n$ (no. 14)	$P2_1/n$ (no. 14)
M.W.	323.68	253.25	241.21
a / Å	15.943(2)	3.872(1)	3.806(1)
b / Å	6.864(1)	11.643(2)	12.203(2)
c / Å	12.957(2)	26.223(5)	23.072(4)
α / º	90	90	90
β / º	111.21(1))	93.52(3)	93.30(1)
γ / º	90	90	90
V / Å^3	1321.9(3)	1179.8(4)	1069.6(3)
Z	4	4	4
D_c /g/cm^{-3}	1.626	1.426	1.498
μ mm^{-1}	0.321	0.101	0.113
Measurement	Bruker APEX II	Bruker APEX II	Bruker APEX II
Measured	13568	5391	10901
Unique reflections,	4148, 0.027-	1431, 0.060	3361, 0.026
Observed	2677	1047	2623
Absorption	*SADABS*	*SADABS*	*SADABS*
T_{min}, T_{max}	0.875, 1.000	0.600, 1.000	0.787, 1.000
R	0.0484	0.0811	0.0625
*wR*2 [all data]	0.1464	0.2339	0.1827

Table 2. DNA binding constants for ligands and complexes. Constants were determined at 25 °C, in PIPES 0.02 M, pH 7.0 (in parenthesis the standard deviations on the last significant figure are reported).

DNA binding constants			
Ligands	**$K_{binding}$ (M^{-1})**	**Copper complexes**	**$K_{binding}$ (M^{-1})**
L1	1.07(1) x 10^6	**C1**	3.55(1) x 10^5
L2	1.4(1) x 10^4	**C2**	1.3(1) x 10^3
L3	5.01(1) x 10^8	**C3**	1.91(1) x 10^5
L4	1.58(1) x 10^8	**C4**	3.31(1) x 10^5
L5	3.16(4) x 10^4	**C5**	4.17(1) x 10^5
L6	4.0(3) x 10^4	**C6**	1.2(1) x 10^3

Table 3. Antiproliferative activity of ligands and complexes against human derived cell lines.

Compound	[a]IC_{50}, μM					
	Human derived tumour cell lines					
	[b]CCRF-CEM	[c]CCRF-SB	[d]SK-MES 1	[e]DU 145	[f]HEP-G2	[g]CRL 7065
L1	>100	>100	>100	>100	>100	>100
L2	>100	20	79	>100	>100	>100
L3	>100	70	>100	>100	>100	>100
L4	>100	>100	>100	>100	>100	>100
L5	58	66	>100	>100	>100	>100
L6	>100	79	>100	>100	>100	>100
C1	96	20	62	>100	>100	>100
C2	41	17	55	>100	>100	52
C3	85	30	67	>100	>100	57
C4	76	19	57	>100	>100	84
C5	36	19	53	>100	>100	>100
C6	56	14	37	>100	79	11

[a]Compound concentration (μM) required to reduce cell proliferation by 50%, as determined by the MTT method, under conditions allowing untreated controls to undergo at least three consecutive rounds of multiplication; [b]human acute T-lymphoblastic leukaemia; [c]human acute B-lymphoblastic leukaemia; [d]human lung carcinoma, [e]human prostate carcinoma; [f]human hepatocellular carcinoma; [g]human normal foreskin.

Table 4. QSAR descriptors calculated with Spartan'14 (density functional B3LYP, 6-31G*)

Cpd	Area ($Å^2$)	Volume ($Å^3$)	PSA[1] ($Å^2$)	Log P[2]	HBA[3]	P-Area[4] ($Å^2$)	Acc. P-Area[5] ($Å^2$)	P.A.[6]	MinElPot[7] (kJ/mol)	MaxElPot[8] (kJ/mol)	HOMO[9] (eV)	LUMO[10] (eV)	EBG[11] (eV)	χ[12] (eV)	η[13] (eV)	S[14] (eV^{-1})	μ[15] (eV)	ω[16]	DM[17] (debye)
L1	235.59	225.72	25.217	2.45	2	45.73	190.21	58.73	-187.32	98.75	-6.14	-2.11	4.03	-2.02	2.02	24.81	-4.13	4.22	4.4
L2	241.22	230.28	25.189	2.61	2	46.82	191.26	59.12	-178.98	111.71	-6.25	-2.30	3.95	-1.98	1.98	25.32	-4.28	4.63	2.55
L3	265.30	252.79	32.107	2.32	3	66.84	207.49	66.84	-196.45	121.29	-5.80	-1.92	3.88	-1.94	1.94	25.77	-3.86	3.84	6.9
L4	265.35	252.84	32.156	2.32	3	61.27	207.71	60.99	-194.00	114.50	-5.86	-2.07	3.79	-1.90	1.90	26.39	-3.97	4.15	5.56
L5	251.26	239.39	25.206	3.01	2	47.68	201.78	59.86	-174.09	112.17	-6.32	-2.36	3.96	-1.98	1.98	25.25	-4.34	4.76	2.11
L6	241.85	230.70	25.577	2.61	2	62.70	191.57	59.14	-217.43	146.94	-6.14	-2.13	4.01	-2.01	2.01	24.94	-4.14	4.26	4.36
C1	480.30	473.44	63.076	-	7	441.21	335.27	-	393.3	715.42	-11.85	-7.91	3.94	-1.97	1.97	25.38	-9.88	24.78	2.04
C2	489.74	482.33	62.604	-	7	450.21	338.58	-	288.24	768.89	-11.74	-7.99	3.75	-1.88	1.88	26.67	-9.87	25.95	4.42
C37O	540.99	527.80	77.605	-	9	498.67	368.58	-	271.40	701.08	-11.00	-7.46	3.54	-1.77	1.77	28.25	-9.23	24.07	2.31
C4 6O	540.71	527.88	77.209	-	0	498.92	369.22	-	254.42	705.67	-10.89	-7.69	3.2	-1.60	1.60	31.25	-9.29	26.97	1.89
C5	512.06	500.71	63.644	-	7	476.70	357.19	-	296.90	727.82	-11.68	-8.07	3.61	-1.81	1.81	27.70	-9.88	27.01	5.87
C6	490.44	482.53	63.469	-	7	450.10	338.55	-	307.47	743.43	-11.75	-7.91	3.84	-1.92	1.92	26.04	-9.83	25.16	2.61

[1]Polar Surface Area; [2]estimated according to [41]; [3]Hydrogen-bond acceptor; [4]polar area; [5]accessible polar area; [6]polarizability; [7]minimum value of the electrostatic potential (as mapped onto an electron density surface); [8]maximum value of the electrostatic potential (as mapped onto an electron density surface), [11]energy band gap, [12]electronegativity, [13]hardness, [14]global softness ($x10^{-2}$), [15]chemical potential, [16]global electrophilicity index, [17]dipole moment.